Computational Nonlinear Least Squares in Electric Current Tomography

N. Mahdavi-Amiri[1] and S.R. Seydnejad[2]

Producing images of cross-sections of a body, or tomography, has applications in medical engineering. We consider the electric current tomography, which has recently attracted some attention. The quantity which plays a key role in representing the picture is the conductivity (or resistivity) of the existing tissues in the cross-section of the body. Electrical current is injected into the body and the voltages of various points of the surrounding environment are measured. The injection of electrical current and the measurement of the voltages are accomplished by certain electrodes around the surface of the section. The distribution of body resistivity is estimated by using the measured voltages. Several computational methods for construction of the image (computing conductivity distributions) are discussed, resulting in optimization models of the nonlinear least squares type. Various numerical techniques for solving the least squares problem are discussed. A system is built to demonstrate the practical usefulness of electric current tomography. The system is tested and useful results are noted.

INTRODUCTION

Much activity has been devoted to the construction of images of cross-sections of a body (or tomography). Recently, electrical impedance tomography (EIT) has attracted some attention. The quantity playing a key role in constructing the image is the resistivity of the cellular tissues around the considered cross-section. To compute the resistivity, sinusoidal electric current is injected into the surrounding area. The flow of the current causes a drop in voltage in various points of the body. Since the surface of the body is most easily accessible, an estimate of the resistivity distribution inside the body is obtained by measuring the voltage of the surface. Injection of the current, voltage measurement and image construction are all carried out under the control of a computer and the connecting electrodes situated within the surrounding area (see Figure 1). To construct the image, one needs to solve certain nonlinear least squares problems. Various schemes for finding numerical solutions of such problems are discussed and contrasted. The effect of some of these techniques in our setting is demonstrated by testing our proposed system.

THE PRINCIPAL RELATION

The flow of electric current having the density $\vec{j}(x,y)$ inside an object with resistivity $P(x,y)$ will cause an electric field $\vec{E}(x,y)$. The follow-

1. Department of Mathematical Sciences, Sharif University of Technology, Tehran, I.R. Iran.
2. Department of Electrical Engineering, Imperial College, London, U.K.

Scientia Iranica, Vol. 1, No. 4, © Sharif University of Technology, January 1995.

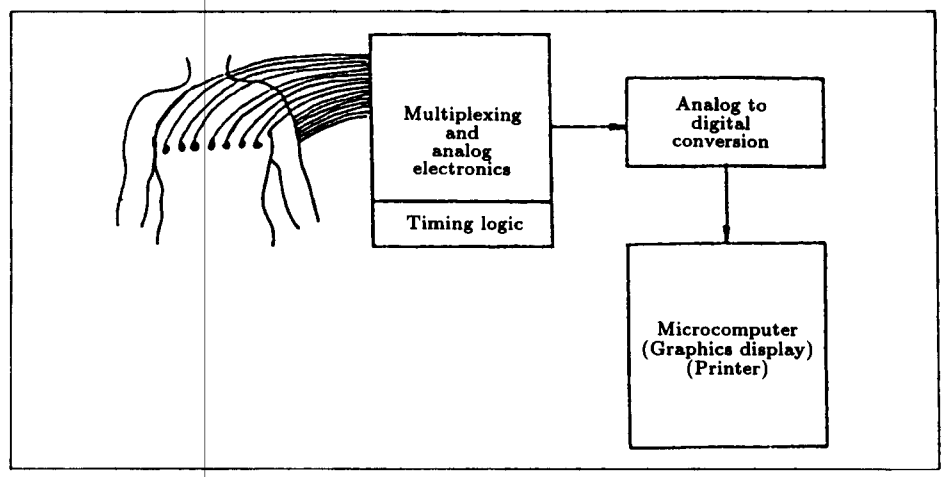

Figure 1. Placement of electrodes for chest tomography.

ing equation is held [1]:

$$\nabla.\vec{j} = \nabla.(\frac{1}{P}\vec{E}) = -\nabla.(\frac{1}{P}\nabla V(x,y)) = 0, \tag{1}$$

where $V(x,y)$ is the electric potential function. Letting j denote the density of the current injected by the electrode, then the following boundary conditions are obtained:

$$\frac{1}{P}\frac{\partial V}{\partial n} = \begin{cases} j & \text{in positive current electrode} \\ -j & \text{in negative current electrode} \\ 0 & \text{otherwise} \end{cases}, \tag{2}$$

where $\frac{\partial V}{\partial n}$ is the derivative of the potential function with respect to the normal direction (the direction perpendicular to the surface area). Thus, Equation 1 with the boundary conditions in Equation 2 must be held. In electrical impedance tomography, we are faced with the inverse problem, measuring the distribution of the current and the potential function around the surface of the cross-section of the body, we are interested in obtaining the resistivity of the section inside. To do this, we indeed solve Equation 1 with boundary conditions in Equation 2 iteratively. In other words, we first assume an initial resistivity distribution $P(x,y)$ for the section and then solve Equation 1. Based on the potential distribution obtained for the surface and its difference from the measurements, and use of a particular iterative method, convergence to the actual solution is accomplished.

THE FINITE ELEMENT METHOD

The differential equation, Equation 1, can be quite complicated in practice and, hence, an analytic solution cannot be hoped for. Thus, we solve Equation 1 numerically by the finite elements method (FEM). To do this, we consider the cross-section as a planar 16 equally-sided polygon divided into 56 triangular elements, as in Figure 2 (increasing the number of elements results in higher accuracy but requires more storage and more time for computations. For practical reasons, we restricted ourselves to 56 elements). We assume that the potential function is linear for each element inside the polygon. Therefore, we will have:

$$V(x,y) = \sum_{e=1}^{56} V_e(x,y)\ , \tag{3}$$

$$V_e(x,y) = \begin{cases} a + bx + cy & \text{inside element } e \\ 0 & \text{otherwise,} \end{cases} \tag{4}$$

where a, b and c are constant scalars. Using the linear functions in Equation 4, one can show that the following relations are held for each

element e [2]:

$$\begin{bmatrix} Y_{11} & Y_{12} & Y_{13} \\ Y_{21} & Y_{22} & Y_{23} \\ Y_{31} & Y_{32} & Y_{33} \end{bmatrix} \begin{bmatrix} V_{e1} \\ V_{e2} \\ V_{e3} \end{bmatrix} = \begin{bmatrix} I_{e1} \\ I_{e2} \\ I_{e3} \end{bmatrix} , \tag{5}$$

where:

$$Y_{ij} = (b_i b_j + c_i c_j)/(2A_e P_e) \ , i \neq j \ , \tag{6}$$

$$\begin{cases} b_1 = y_2 - y_3 \ , & b_2 = y_3 - y_1 \ , \\ b_3 = y_1 - y_2 \ , & \\ c_1 = x_3 - x_2 \ , & c_2 = x_1 - x_3 \ , \\ c_3 = x_2 - x_1 \ , & \end{cases} \tag{7}$$

$$\begin{cases} Y_{11} = -Y_{12} - Y_{13} \ , & Y_{22} = -Y_{21} - Y_{23} \ , \\ Y_{33} = -Y_{31} - Y_{32} \ , & \\ Y_{ij} = Y_{ji} \ , & i,j = 1,2,3 \ , \end{cases} \tag{8}$$

with the following definitions:

P_e = resistivity of element e (assumed constant within the element),

V_{ei} = potential of vertex i of element e,

x_i, y_i = plane coordinates of vertex i of element e,

A_e = area of element e,

$R_{ij} \triangleq \frac{1}{Y_{ij}}$ = electrical resistivity between vertices i and j $(i \neq j)$ of element e,

I_{ei} = electrical current entered into vertex i of element e.

Thus, it is shown that the FEM approximation for a triangular element having resistivity P_e is identical with a triangular electric resistance network [3]. For the exact solution of Equation 1, we need to know the current and potential distributions on the entire section of the body. However, we can only have a finite number of measurements in practice. Furthermore, the accuracy obtained in the measurements is limited by the number of electrodes being used. It can be shown that for N electrodes, the number of possible independent measurements would be $N(N-3)/2$ [4]. For our computer simulation, we chose 16 electrodes.

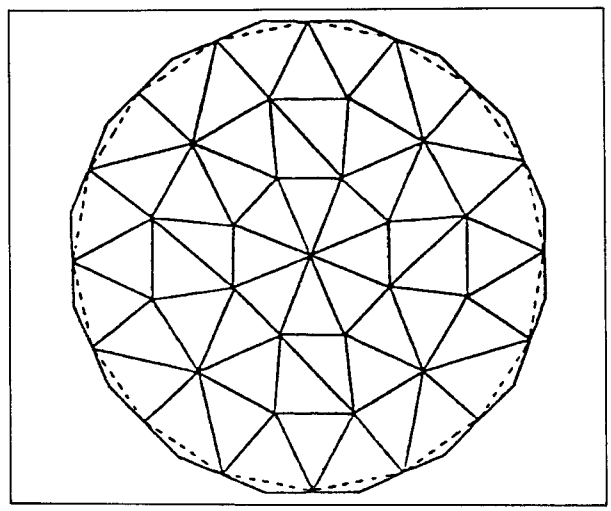

Figure 2. A 16 equally-sided polygon with 56 elements.

THE LEAST SQUARES MODEL

There are a number of methods for computing the resistivity distribution. One technique is based on minimizing the error (the difference between the measured voltages and their estimates obtained in the iterative process) in a particular norm. Using the Euclidean norm (or 2-norm) we obtain the nonlinear least squares problem:

$$\begin{aligned} \textit{minimize } K(P) &\triangleq \frac{1}{2}\|\underline{f}(P) - \underline{V_0}\|_2^2 \\ &= \frac{1}{2}(\underline{f}(P) - \underline{V_0})^T(\underline{f}(P) - \underline{V_0}) \ , \end{aligned} \tag{9}$$

where $\underline{V_0} = [v_{01}, v_{02}, \ldots, v_{0L}]^T$ is the vector of measured voltages, $P = [p_1, p_2, \ldots, p_M]^T$ is the vector of resistivities corresponding to the elements, and $\underline{f}(P) = [f_1, f_2, \ldots, f_L]^T$ is the vector of computed voltages which is a function of resistivities. The necessary conditions for the solution of the above problem are that the gradient of $K(P)$ must vanish at the solution [5,6]. Hence, we have:

$$K'(P) = [f'(P)]^T(\underline{f}(P) - \underline{V_0}) = 0 \ , \tag{10}$$

where the L by M matrix $f'(P)$ is the Jacobian of $\underline{f}(P)$:

$$[f'(P)]_{ij} = \frac{\partial f_i(P)}{\partial p_j} . \quad (11)$$

We note here that the model in Problem 9 may be supplemented to include constraints on P. The simplest, of course, is the nonnegativities of resistivities. Constrained optimization problems need to be handled differently [6]. However, for our problem we do not find the added complication necessary, since a good initial estimate for resistivities is often available and, hence, the subsequent iterates would remain nonnegative. Next, we turn into a discussion of various methods for solving Problem 9.

METHODS OF SOLUTION

Numerical methods for solving Problem 9 are focused on finding a solution of the nonlinear Equation 10. Nonlinear equations are usually solved by an iterative process based on a linear approximation (to follow Newton's approach). The linear approximation of Equation 10 is as follows:

$$K'(P_{(k+1)}) \approx K'(P_{(k)}) + K''(P_{(k)})\triangle P_{(k)} = 0 , \quad (12)$$

where K'', the Hessian of $K(P)$, is as follows:

$$K'' \triangleq f'^T f' + \sum_{i=1}^{L} (f_i - v_{0i}) \cdot \nabla^2 (f_i - v_{0i}) . \quad (13)$$

Having $P_{(k)}$, an estimate of the resistivity vector, at hand, $\triangle P_{(k)}$ is obtained by solving Equation 12. Thus, we need to solve the following linear system of equations for $\triangle P_{(k)}$:

$$K''(P_{(k)})\triangle P_{(k)} = -K'(P_{(k)}) . \quad (14)$$

The new estimate can then be defined as:

$$P_{(k+1)} = P_{(k)} + \triangle P_{(k)} . \quad (15)$$

We note that, when far from a solution of Problem 9, the updating scheme in Equation 15 may not be satisfactory. In situations like this, one usually performs a line search to find a parameter $\alpha_k, 0 < \alpha_k \leq 1$, so that $P_{(k+1)} = P_{(k)} + \alpha_k \triangle P_{(k)}$ is approximately a minimizer (with respect to α) of $K(P_{(k)} + \alpha \triangle P_{(k)})$ [5,6]. For our purposes, the simplified version in Equation 15 turns out to be satisfactory.

We are now ready to propose an algorithm for solving the inverse problem.

(a) Inject the electric current into the section of the body and measure the voltages on the surface of the body.

(b) Divide the section of the body into M triangular elements ($M < L$) and initialize the resistivity vector to some arbitrary (nonnegative) numbers (this is the initial P, say $P_{(0)}$). Set k to 0.

(c) Based on $P_{(k)}$ and using the FEM, compute $\underline{f}(P_{(k)})$ and $f'(P_{(k)})$.

(d) Solve the system of Equation 14 to compute $\triangle P_{(k)}$.

(e) Let $P_{(k+1)} = P_{(k)} + \triangle P_{(k)}$.

(f) If convergence criteria is met then stop.

(g) Let $k = k + 1$. Go to step (c).

Steps (c) and (f) of the algorithm need some comment. In step (c), since the FEM approximation turns the section of the body into an electric resistance network, the computations of $\underline{f}(P)$ and $f'(P)$ are made easily possible [4]. For convergence criteria in step (f), one may set a predetermined tolerance level for the acceptance of the approximated error in the solution, the difference between the measured and the computed voltages. Based on the tolerance level, the convergence criteria may be set by choosing a norm, say the Euclidean, for the difference vector.

The Gauss-Newton Method

The key numerical step of our concern in the algorithm is step (d). Various methods propose different ways for solving Equation 14. From Equation 13, we realize that the exact Hessian

consists of two terms, the first being that $f'^T f'$ is available, and the second (the summation) requiring second order information concerning $(f_i - v_{0i})$ for all i. One method, the Gauss-Newton [7-9], disregards the second term altogether and uses the approximation:

$$K'' \approx f'^T f' . \tag{16}$$

Using K'' as Equation 16, and using Equation 10, Equation 14 turns to:

$$[f'(P_{(k)})]^T f'(P_{(k)}) \triangle P_{(k)} = - [f'(P_{(k)})]^T \, [\underline{f}(P_{(k)}) - \underline{V_0}] , \tag{17}$$

which may be used as an approximation to Equation 14 in step (d).

The Jacobian matrix plays an important role in the solution of the inverse problem. The components of this matrix are the derivatives of voltages with respect to resistivity of the elements. It is clear that the low accuracy in the Jacobian matrix would result in an unreliable picture, since this would mean low sensitivity of the measured voltages with respect to the resistivities. Unfortunately, the closer the element is to the center of the section the less reliable the picture becomes (due to the low sensitivities). But, reliable images are needed.

One remedy is to increase the number of the elements. This, of course, would mean less area for each element and, hence, more work may be required to obtain the image. In general, the matrix $[f'(P)]^T[f'(P)]$ may be ill-conditioned (this is certainly true when the Jacobian matrix is rank deficient or close to a rank deficient one). This is the situation where the Gauss-Newton method may not converge to a solution (or the convergence may be too slow for any practical purpose), especially when the initial point may fall far from the solution. Although, for our purposes we can always start with a good initial point, solving the system in Equation 17 would still have numerical difficulties when it is badly conditioned. To solve this difficulty, regularization techniques have been suggested, which we discuss below.

The Levenberg-Marquardt Method

Instead of minimization of $K(P)$ as in Problem 9, one, for example, suggests the minimization of a penalized model [10]:

$$K(P) = \frac{1}{2}\|\underline{f}(P) - \underline{V_0}\|_2^2 + \frac{1}{2} r G(P) , \tag{18}$$

when r is a constant positive scalar and $G(P)$ is a nonnegative function of P. Usually, $G(P)$ is taken to be a quadratic term of form:

$$G(P) \triangleq P^T H P , \tag{19}$$

for some positive definite matrix H. It is now easy to see that the system in Equation 17 becomes:

$$\{[f'(P_{(k)})]^T f'(P_{(k)}) + rH\} \triangle P_{(k)} = -[f'(P_{(k)})]^T [\underline{f}(P_{(k)}) - \underline{V_0}] . \tag{20}$$

If we choose $H = I$, then the resulting method is what is called the Levenberg and Marquardt method for solving nonlinear least squares models [11,12]. We realize that the approximation matrix rI is effectively being used in place of the second term in Hessian, given by Equation 13. For our problem, the second term of the Hessian at the solution must vanish, so large values for r may not cause convergence to the solution, or at least slow down the convergence rate. On the other hand, small values of r may cause divergence from the solution. Our suggestion, arrived at from numerical experiments, is to use $r = \frac{1}{10}$ at the initial point and reduce it by the factor $\frac{1}{10}$ after each iteration (penalized models are very common in constrained nonlinear optimization. For general discussions, see [6]). There should be rooms for improvement in the way of choosing r and its subsequent reductions.

Recent developments for solving nonlinear least squares problems propose more accurate approximations for the summation term in Equation 13. These methods are named as "secant" or "quasi-Newton". They are based on secant approximation of the second order terms in the summation, either individually or

collectively. We tried these methods based on the material in [13,14]. Since our computational results do not present superiority of these techniques for the problem at hand, we will not elaborate on them here any further (we note, however, that they are as competitive as the other methods mentioned before). We feel that further work on secant methods for our problem may prove promising.

The Weighted Methods

Any of the above methods may be applied to a weighted least squares form:

$$minimize\ K(P) = \frac{1}{2}\|W(\underline{f}(P) - \underline{V_0})\|_2^2 , \tag{21}$$

where W is the weight matrix :

$$W = \begin{bmatrix} w_{11} & & & 0 \\ & w_{22} & & \\ & & \ddots & \\ 0 & & & w_{LL} \end{bmatrix},$$

where $w_{ii} \geq 0, 1 \leq i \leq L$ and $\sum_{i=1}^{L} w_{ii} = 1$. This model would permit the assignment of a separate weight to the voltage corresponding to each element (the original model in Problem 9 considers equal weights of 1 for all the elements inherently). This new model may be more meaningful in situations where the sensitivities of certain elements are considered higher than others, or where the presence of noise in the system is considered to be more damaging to some elements. With this viewpoint, it can be shown that the Gauss-Newton version for solving Problem 21 becomes the solution for the system of equations:

$$[f'^T W^2 f']\triangle P_{(k)} = -f'^T W^2(\underline{f} - \underline{V_0}) , \tag{22}$$

and the Levenberg-Marquardt method would result in solving the system:

$$[f'^T W^2 f' + rI]\triangle P_{(k)} = -f'^T W^2(\underline{f} - \underline{V_0}) . \tag{23}$$

We choose the weights to compensate for possible damage in the presence of noise. That is, we assume that the less the measured voltage, the more sensitive it will become to the noise in the system, and, hence, a smaller weight is assigned to it. For computational purposes, we first normalize the vector of voltages and then the individual weights are taken to be the ratios obtained as the absolute values of the corresponding normalized components to the overall sum of the components.

PRACTICAL RESULTS

A 16-sided polygon phantom having a diameter of 12.5 cm and height of 2.5 cm has been used. The phantom is filled with a saline solution having a resistivity of 65% ohm-meter. Figure 3 illustrates the constructed image of the phantom filled with the solution. Figures 4 and 5 show the constructed image after the insertion of a cylinder (marked with broken lines). In Figure 4, a glass cylinder having a diameter of 3.5 cm has been dropped, while the one in Figure 5 is a metal cylinder with 3 cm diameter. These results have been presented in [15]. Some of the main factors for the introduction of errors in producing the image are reported possibly as: (1) the use of a small number of elements for the FEM, (2) the actual 3-dimensional shape of the phantom while the presentation here is based on a 2-dimensional analysis, (3) the existence of noise and error in the electronic system being used, and (4) error in construction of the phantom.

CONCLUSIONS

For constructing electrical impedance images, an approximate electrical resistance network for the considered section of the body is obtained by an FEM approximation. Then, starting with an initial estimate of the resistivity distribution of the section, an iterative process is developed to find the resistivities so that the difference between the measured and computed voltages is minimized in the least squares sense. Various nonlinear least squares methods are

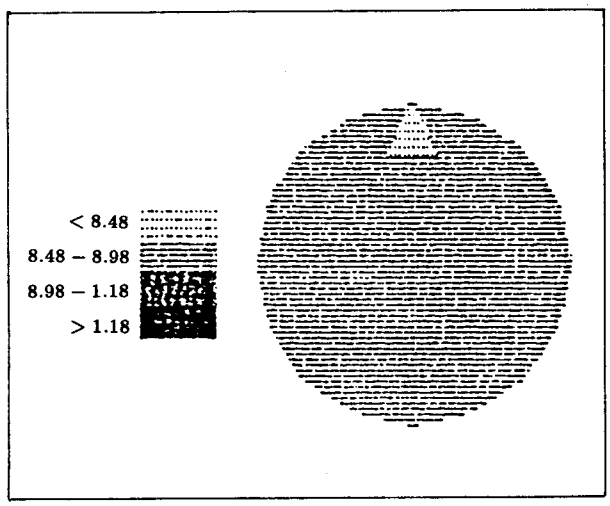

Figure 3. Constructed image of the phantom having a salt-water solution.

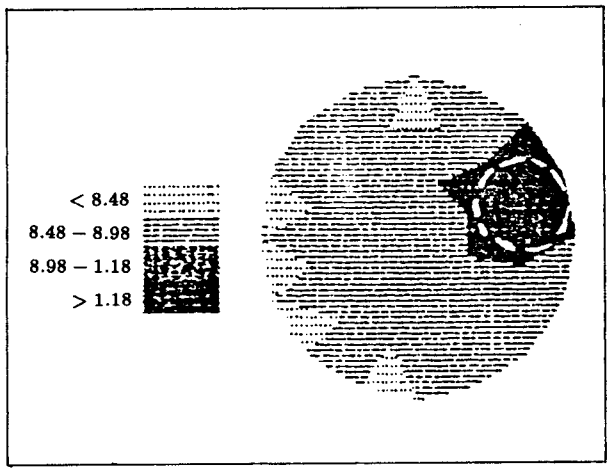

Figure 4. Constructed image with the presence of glass cylinder (the broken lines mark the actual position of the cylinder).

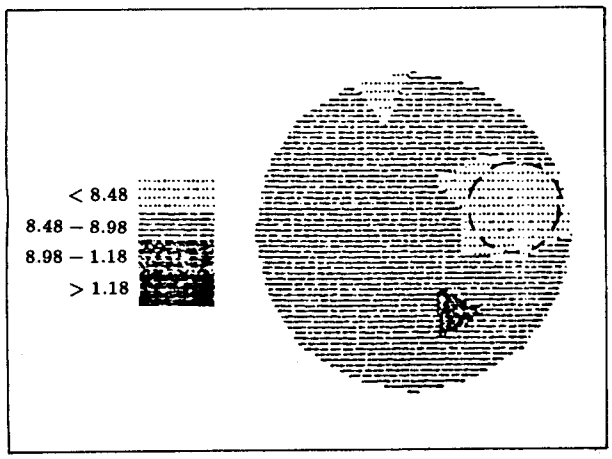

Figure 5. Constructed image with the presence of metal cylinder.

discussed and used in the computations. It is found that the Jacobian matrix of the vector function of voltages plays a significant role in the convergence behavior of a method to the solution. Various techniques as possible ways for improving the speed of convergence to the solution have been suggested.

REFERENCES

1. Hayt, W.H. *Engineering Electromagnetics*, McGraw-Hill Co. (1981).

2. Murai, T. "Electrical impedance computed tomography based on a finite element model", *IEEE Transactions on Biomedical Engineering*, pp 177-184 (March 1985).

3. Chua, L. *Linear and Nonlinear Circuits*, McGraw-Hill Co. (1987).

4. Seydnejad, S.R. "Electric current tomography", Master's thesis (in Farsi), Sharif University of Technology, Tehran, I.R. Iran (1992).

5. Dennis, J.E., Jr. and Schnabel, R. *Numerical Methods for Unconstrained Optimization and Nonlinear Equations*, Prentice-Hall (1983).

6. Fletcher, R. *Practical Methods of Optimization*, 2nd Edn., John Wiley and Sons (1987).

7. Dennis, J.E., Jr. "Nonlinear least squares and equations", in *The State of the Art of Numerical Analysis*, D. Jacobs, Ed., Academic Press, Orlando, FL, USA (1977).

8. Gill, P.E. and Murray, W. "Algorithms for the solution of the nonlinear least squares problem", *SIAM J. on Numerical Analysis*, **15**(5), pp 977-992 (1978).

9. Wedin, P.A. "On the Gauss-Newton method for the nonlinear least squares problem", ITM Arbestrapport No. 24, Institute for Tellampad Matematik, Stockholm, Sweden (1974).

10. Jacobs, D. *The State of the Art in Numerical Analysis*, Academic Press (1977).

11. Levenberg, K. "A method for the solution of certain problems in least squares", *Q. Appl. Math.*, **2**, pp 164-168 (1944).

12. Marquardt, D. "An algorithm for least squares estimation for nonlinear parameters", *SIAM J. on Applied Mathematics*, **11**, pp 431-441 (1963).

13. Dennis, J.E., Jr., Gay, D.M. and Welsch, R.E. "An adaptive nonlinear least squares algorithm", *ACM Transactions on Mathematical Software*, **7**(3), pp 348-368 (1981).

14. Mahdavi-Amiri, N. and Bartels, R.H. "Constrained nonlinear least squares: an exact penalty approach with projected structured quasi-Newton update", *ACM Transactions on Mathematical Software*, **15**(3), pp 220-242 (1989).

15. Seydnejad, S.R. and Mahdavi-Amiri, N. "Optimization in electric current tomography", in *Proceedings of the International Congress on Computational Methods in Engineering*, M.A. Yaghoubi, Ed., **1**, Shiraz University, Shiraz, I.R. Iran, pp 51-58 (May 1993).